



ELSEVIER



<https://doi.org/10.1016/j.ultrasmedbio.2020.08.023>

● Original Contribution

COMPREHENSIVE VISCOELASTIC CHARACTERIZATION OF TISSUES AND THE INTER-RELATIONSHIP OF SHEAR WAVE (GROUP AND PHASE) VELOCITY, ATTENUATION AND DISPERSION

JUVENAL ORMACHEA, and KEVIN J. PARKER

Department of Electrical and Computer Engineering, University of Rochester, Rochester, New York, USA

(Received 21 May 2020; revised 21 August 2020; in final from 22 August 2020)

Abstract—We report shear wave phase and group velocity, dispersion and attenuation in oil-in-gelatin viscoelastic phantoms and *in vivo* liver data. Moreover, we measured the power law coefficient from each dispersion curve and used it, together with the shear wave velocity, to calculate an approximate value for attenuation that agrees with independent attenuation measurements. Results in phantoms exhibit good agreement for all parameters with respect to independent mechanical measurements. For *in vivo* data, the livers of 20 patients were scanned. Results were compared with pathology scores obtained from liver biopsies. Across these cases, increases in shear wave dispersion and attenuation were related to increased steatosis score. It was found that shear wave dispersion and attenuation are experimentally linked, consistent with simple predictions based on the rheology of tissues, and can be used individually or jointly to assess tissue viscosity. Thus, this study indicates the possible utility of using shear wave dispersion and attenuation to non-invasively and quantitatively assess steatosis. (E-mail: jormache@ur.rochester.edu) © 2020 World Federation for Ultrasound in Medicine & Biology. All rights reserved.

Key Words: Elastography, Viscoelasticity, Dispersion, Attenuation, Power law, Steatosis, Shear waves.

INTRODUCTION

Shear wave elastography (SWE) has had success in measuring liver stiffness, which is correlated with higher grades of liver fibrosis. However, the assessment of viscosity and its correlation with liver steatosis is still an area of active research. Thus, there is need for a non-invasive and readily available method to quantify steatosis and other liver conditions.

Different approaches to measurement of the viscoelastic properties of the liver are becoming available to clinicians, many involving shear waves. The additional parameters that can now be measured with SWE include shear wave dispersion (SWD) and attenuation (SWA). By the use of acoustic radiation force (ARF)-based methods, SWD can be calculated by measuring the linear slope of the phase velocity over a frequency range. The phase velocity is extracted from the phase shift of the shear waves (Chen et al. 2004; Deffieux et al. 2009) over distance. Alternatively phase velocity can be estimated by finding

the maximum amplitude at a spatial frequency $k(w)$ for each discrete temporal frequency within the 2-D Fourier transform of the shear wave history (Baddour 2011, 2012; Nenadic et al. 2013; Nightingale et al. 2015; Kumar et al. 2018). Trout et al. (2020) found that SWD was associated with viscosity and was lower in adults compared with children. Sugimoto et al. (2018) found that lobular inflammation in liver is correlated with SWD. Later, Sugimoto et al. (2020) reported that shear wave speed (SWS) closely correlates with the degree of fibrosis, but SWD better predicts the degree of necro-inflammation.

Alternatively, SWA can be derived from the analytical solution in cylindrical coordinates to an asymmetric push pulse (Parker et al. 2018c), recovered from the phase and amplitude decay versus distance (Budelli et al. 2017) or using a spatial frequency broadening measuring method (Nenadic et al. 2017). In a clinical study, Sharma et al. (2019) found that SWA increases with higher stages of steatosis. This supports their hypothesis regarding the increase in attenuation with increasing addition of fat and indicates the possible utility of the measurements for non-invasive and quantitative assessment of steatosis. Nenadic et al. (2017) concluded that liver transplant rejection cases had a lower SWA than

Address correspondence to: Juvenal Ormachea, Department of Electrical and Computer Engineering, University of Rochester, 731 Computer Studies Building, Box 270231, Rochester, NY 14627-0231. E-mail: jormache@ur.rochester.edu

normal livers. Budelli et al. (2017) measured the SWA in phantoms and *in vivo* liver with good correlation using two different techniques, supersonic shear imaging and transient elastography.

Given the rapidly expanding set of estimated parameters and sometimes discordant results, it can be overlooked that there are deep theoretical relations linking fundamentals of causal waves, including shear waves in tissues. Generally, the constraints of causality create strong links between the frequency dispersion of phase velocity (dispersion) and frequency-dependent attenuation. These are captured succinctly by Kramers–Kronig relations (Futterman 1962; Waters et al. 2000, 2005; Mobley et al. 2003) or Hilbert transform relations (Papoulis 1987). In our context, the specific relationships depend on the particular stress–strain relations that apply to the tissues; in other words, the rheological model that is appropriate for tissues will set the particular form of the inter-relationship between shear wave phase velocity dispersion and frequency-dependent attenuation. It is germane to point out that some clinical studies (Chen and Holm 2003; Zhang et al. 2007; Urban et al. 2017; Parker et al. 2018a, 2018b) have found that many soft tissues exhibit a SWS with a power law behavior. Within the framework of a power law rheological model, SWD is linked to SWA in a particularly simple way consistent with the Kramers–Kronig relations (Szabo 1995; Waters et al. 2000; Chen and Holm 2003; Parker 2014; Holm 2019). Thus, from physics we know that the dispersion of phase velocity in an individual liver should be directly linked to the lossy, attenuating nature of the tissue, and, for the specific case of power law models of tissue, it is reasonable to estimate the power law coefficient, which is directly related to the SWD and SWA (Parker et al. 2018b, 2018c). To assess the practical and clinical implications of these inter-relationships, this study used custom-made oil-in-gelatin viscoelastic phantoms and *in vivo* liver data collected for previous studies (Parker et al. 2018b, 2018c; Sharma et al. 2019), respectively, and independently measured the shear wave (group and phase velocity, dispersion and attenuation) for a complete viscoelastic characterization. Moreover, this study validates the power law model assumption by measuring their corresponding power law coefficient (PLC), and then used this parameter to approximate the SWA based on the SWS (group and phase) and PLC results.

METHODS

Ultrasound system

A Samsung ultrasound system (Model RS85, Samsung Medison, Seoul, South Korea) and a curved array ultrasound transducer (Model CAI_7 A, Samsung Medison) were used

to produce push beams and track the induced displacements. In these experiments, fewer than 100 central elements of the transducer were used to transmit focused push beams (center frequency = 2.5 MHz, 130- μ s push duration, multifocal depth operation with four sequential pushes along an axial line at regular spacings over 30 mm of increasing focal depth). For a 60-mm focus, the f -number is approximately 1.3. The sampling frame rate was 7.5 kHz. After push transmission, the Samsung system immediately switched to plane wave imaging mode using 135 transducer elements (center frequency = 2.5 MHz). The sampling frequency was set to 20 MHz. Some averaging over depth and noise reduction filtering are applied to the displacement estimates; the precise details are proprietary to Samsung.

Elastography measurements: SWS (group and phase), SWA, SWD and PLC

Displacement waveforms were tracked over time. SWS and SWA coefficients were obtained using the Fourier transform theorems applied to the wave equations reported in Parker and Baddour (2014) and Parker et al. (2018c). The decay of the waveforms' frequency content was analyzed to estimate SWA as a linear (first power) function of frequency, with the value at 150 Hz selected for reporting. Further details on the estimators of attenuation are found in Parker et al. (2018c).

The phase velocity was obtained by calculating the 2-D Fourier transform from the particle velocity signals and finding the maximum amplitude at spatial frequency $k(\omega)$ for each discrete temporal frequency (Nenadic et al. 2013; Nightingale et al. 2015; Kumar et al. 2018). Then, a linear dispersion slope over a specific frequency range was calculated using

$$c_p(f) = \frac{2\pi f}{k} \quad (1)$$

$$c_p(f) = c_0 + \left. \frac{dc}{df} \right|_{f_0} f \quad (2)$$

where c_0 is the intercept at zero frequency, f is frequency and $\left. \frac{dc}{df} \right|_{f_0}$ is the linear dispersion slope evaluated at a particular frequency band around f_0 . Under most rheological models, the linear dispersion slope will be a strong function of frequency, and therefore, comparisons between different results are limited to those closely matched in frequency.

Finally, the PLC was measured from the phase velocity information. For many types of waves (Graff 1975), the group velocity $v_p(\omega)$ governs the propagation of the observed wave packet that is composed of multiple frequencies, and it is related to the phase velocity by

$$v_p(\omega) = \frac{d\omega}{d\beta} \quad (3)$$

where

$$\beta(\omega) = \frac{\omega}{c_p(\omega)} \quad (4)$$

and then, for power law materials (Parker et al. 2018b), the phase velocity $c_p(\omega)$ is defined as

$$c_p(\omega) = c_1 \omega^a \quad (5)$$

where

$$\alpha = \frac{\omega^{(1-a)}}{c_1} \left(\frac{\pi a}{8} \right) \quad (6)$$

and where c_1 is the phase velocity measured at a reference point; for example, at $\omega = 1$ rad/s, a is the power law coefficient and α is the approximate SWA coefficient. Equations (5) and (6) comprise two equations and four unknowns: c_p , a , α and c_1 . Thus, estimates of any two can be used to calculate the other two, producing a complete characterization of the material under the power law model. In Figures 1 and 2 are dispersion curves for different oil-in-gel phantoms and *in vivo* liver tissue, respectively. Both images indicate the specific frequency ranges used for each case to estimate the SWD, PLC and SWA parameters. The frequency ranges

correspond to the mean frequency peak and the -6 -dB criteria of the spectrum signals, respectively. Another observation in the dispersion curves is related to the non-linear behavior at lower frequencies (<70 Hz approximately), and this may be owing to the roll-off of the 2-D Fourier transform signal at low frequencies as explained by Nightingale et al. (2015).

Phantom study

Custom-made castor oil phantoms. Seven different concentrations of oil-in-gelatin phantoms were created. The specific details and procedure for the phantom preparation can be found in Parker et al. (2018a). All experiments were performed 1 d after the phantom preparation to avoid long-term instability issues with the phantoms.

Mechanical measurements for the custom oil-in-gelatin phantoms for comparison purposes. The specific details of the mechanical measurements were described in Parker et al. (2018b). These conventional mechanical measurements were considered the reference when assessing the viscoelastic properties of these oil-

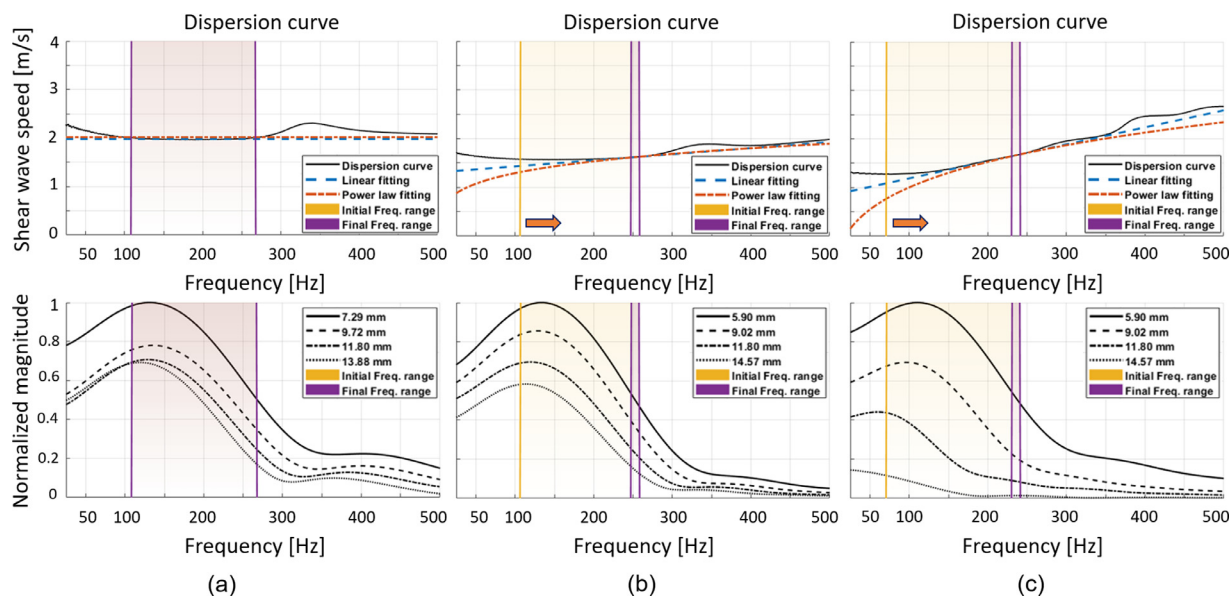


Fig. 1. Phase velocity as a function of frequency extracted from the particle velocity signals using the method described by Nenadic et al. (2013) and its corresponding spectrum signals (taken at different lateral positions) below each dispersion curve plot. The initial frequency range used for estimating shear wave dispersion (SWD), power law coefficient (PLC) and shear wave attenuation (SWA) is shaded in yellow. The minimum (f_{\min}) and maximum (f_{\max}) frequency range values correspond to the mean frequency peak and the -6 -dB criteria of the spectrum signals, respectively. The frequency range dynamically changes until correlation fitting parameters are ≥ 0.85 for both linear and power law curve fittings. The orange arrow represents how the search moved to find a better fitting, and the purple-shaded region indicates the final frequency range. In dispersion curves, the blue dashed lines denote the linear fitting, and the red dashed lines denote the power law fitting. Examples correspond to oil-in-gel phantoms with 2% (a), 18% (b) and 36% (c) castor oil. As noted, as the oil percentage increases, the particle velocity waveform is extended, resulting in a narrower bandwidth in the corresponding spectra.

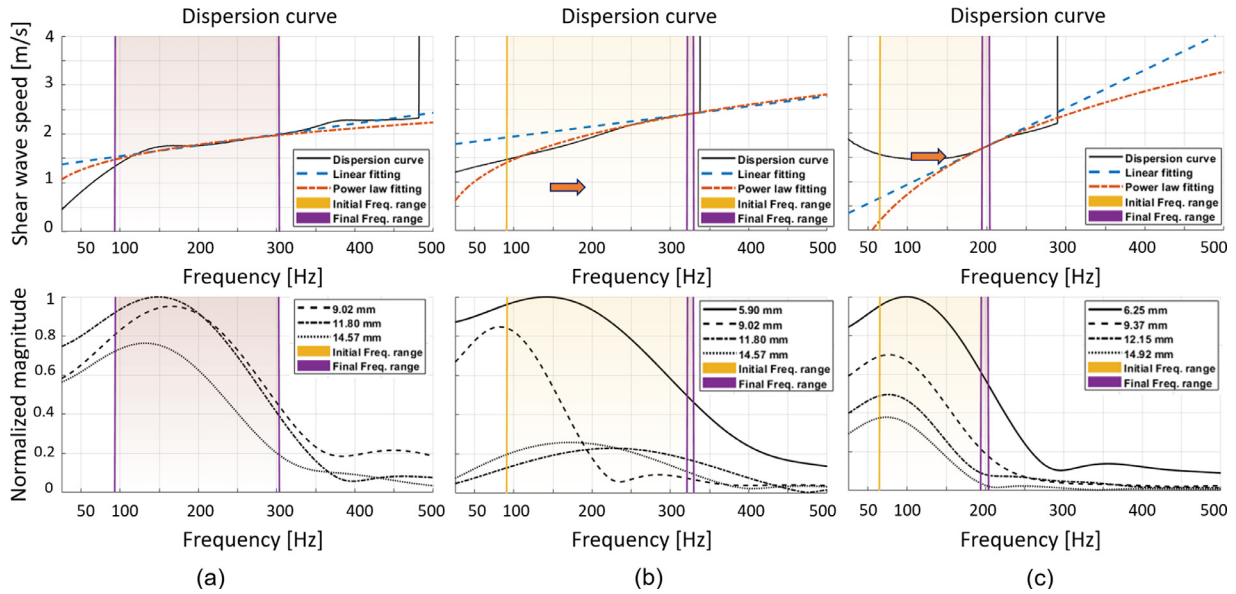


Fig. 2. Phase velocity as a function of frequency extracted from the particle velocity signals using the method described by Nenadic et al. (2013) and the corresponding spectrum signals (taken at different lateral positions) below each dispersion curve plot. The initial frequency range used for estimating shear wave dispersion (SWD), power law coefficient (PLC) and shear wave attenuation (SWA) is shaded in yellow. The minimum (f_{min}) and maximum (f_{max}) frequency range values correspond to the mean frequency peak and the -6 -dB criteria of the spectrum signals, respectively. The frequency range dynamically changes until correlation fitting parameters are ≥ 0.85 for both linear and power law curve fittings. The orange arrow represents how the search moved to find a better fitting, and the purple-shaded region represents the final frequency range. In dispersion curves, the blue dashed lines denote the linear fitting, and the red dashed lines denote the power law fitting. Examples correspond to *in vivo* liver tissue with steatosis scores of S0 (a), S1 (b) and S3 (c). As in Figure 1, as the viscosity increases because of the presence of more fat in liver; the particle velocity waveform is extended, resulting in a narrower bandwidth in the corresponding spectra.

in-gelatin phantoms. As in Zhang et al. (2007) and Ormachea et al. (2016), the stress relaxation curve of each sample was fitted to the Kelvin–Voigt fractional derivative (KVFD) model using standard non-linear

least-squares procedures. This viscoelastic model contains three parameters: E_0 , ζ and τ . E_0 refers to the relaxed elastic constant, ζ to the viscoelastic parameter and τ to the order of fractional derivative. The complex

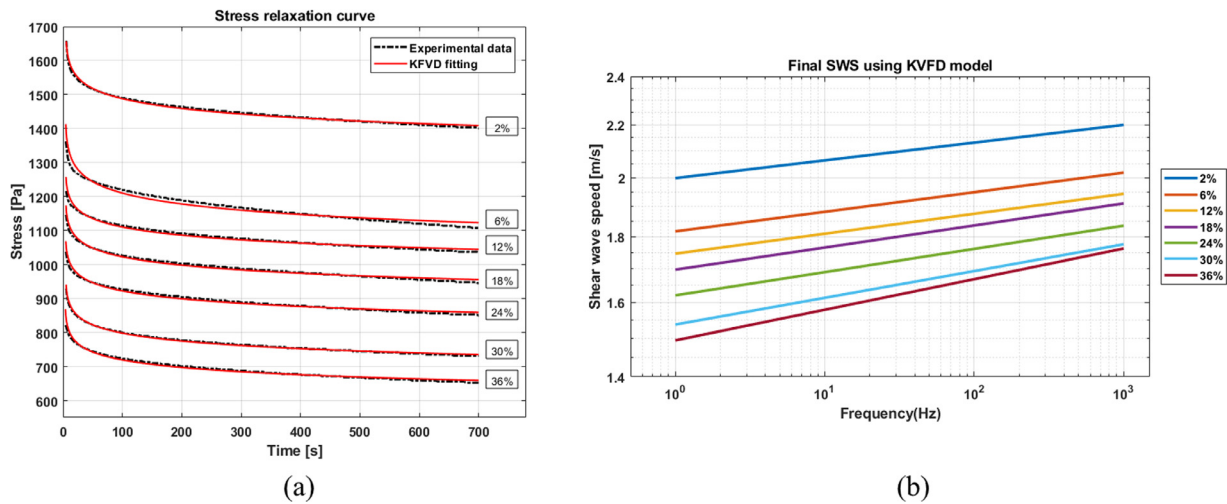


Fig. 3. (a) Stress relaxation measurements in homogeneous viscoelastic phantoms. The boxes indicate the castor oil concentration and the corresponding fitted curves using the Kelvin–Voigt fractional derivative (KVFD) model. (b) Phase velocity as a function of frequency in log–log scale using the estimated KVFD parameter results. It can be noted that for higher oil concentration, the dispersion slope tends to be higher.

Table 1. Trends for SWS, SWD, PLC and SWA as a function of pathology grade

Coefficient	SWS		SWD		PLC		SWA	
	Fibrosis	Steatosis	Fibrosis	Steatosis	Fibrosis	Steatosis	Fibrosis	Steatosis
Spearman	0.66	-0.21	-0.08	0.42	-0.23	0.47	-0.37	0.52
Pearson	0.69	-0.19	-0.04	0.75	-0.12	0.61	-0.30	0.65

PLC = power law coefficient; SWA = shear wave attenuation; SWD = shear wave dispersion; SWS = shear wave speed.

modulus $E^*(\omega)$ is given by

$$E^*(\omega) = \left[E_0 + \zeta \cos\left(\frac{\pi\tau}{2}\right) \omega^\tau \right] + j \left[\zeta \sin\left(\frac{\pi\tau}{2}\right) \omega^\tau \right] \quad (7)$$

From our stress relaxation data, the curve-fit model parameters E_0 , ζ and τ were then used to predict the biomechanical properties. Note that in many tissue measurements where $E_0 \approx 0$, the KVFD model reduces to a two-parameter power law model (Parker et al. 2019). From eqn (7), the phase velocity and SWA coefficient can be obtained using

$$\frac{\omega}{\sqrt{\frac{E^*(\omega)}{3\rho}}} = \frac{\omega}{c_p} - j\alpha \quad (8)$$

where ρ indicates the density of the medium, which is approximately 1000 kg/m^3 in soft tissues. In Figure 3 are

the stress–relaxation curves obtained for each sample and their corresponding fitting, applying the KVFD model, and their corresponding dispersion curves using the fitted results parameters.

Clinical study

Patient enrollment and histology. The Samsung RS85 system was used on patients under the requirements of informed consent and approval from the University of Rochester Research Subjects Review Board. The specific clinical details are described in Sharma et al. (2019). For the 20 adults studied, the average age was 55.1 y, and the average body mass index was 30.5.

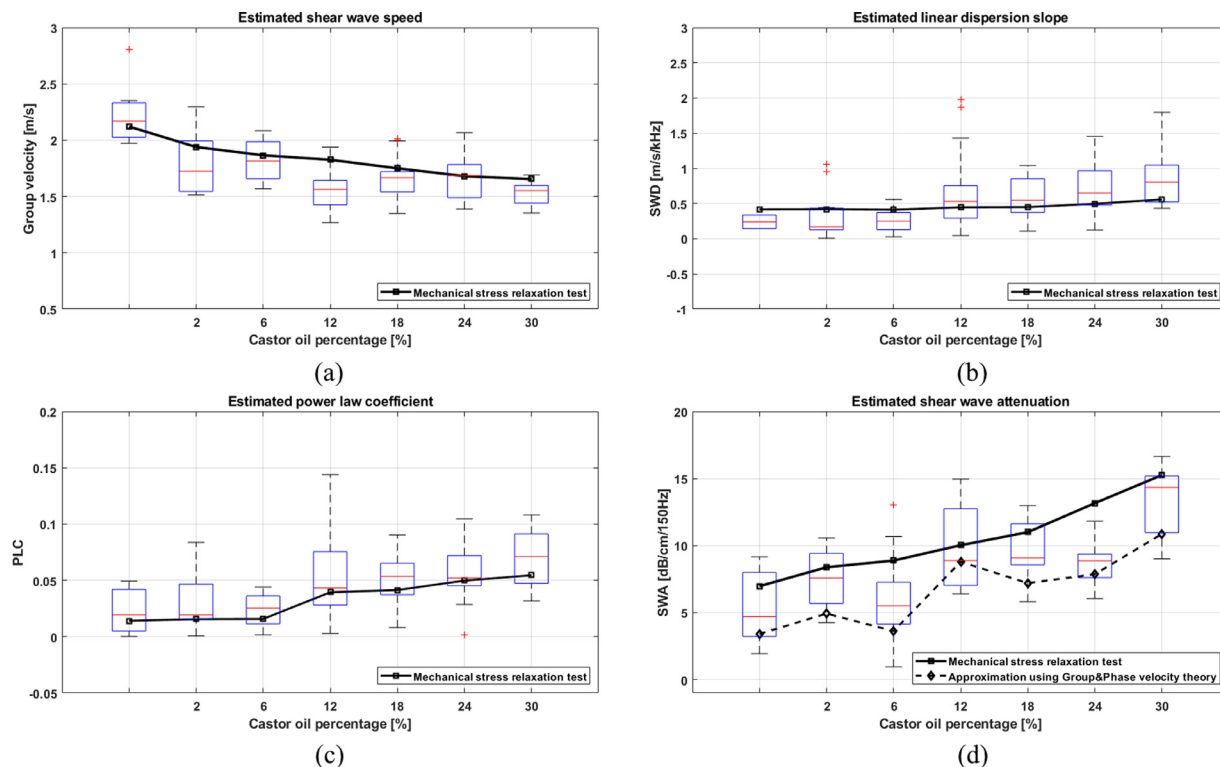


Fig. 4. Shear wave speed (SWS) (a), shear wave dispersion (SWD) (b), power law coefficient (PLC) (c) and shear wave attenuation (SWA) (d) results versus castor oil percentage. The black line corresponds to results extracted for the KVFD model using curve fits to the mechanical stress relaxation data. The black dashed line in (d) represents the SWA approximation using the SWS and mean PLC obtained from the SWE measurements. The independent measurements exhibit reasonable agreement for all cases.

The liver biopsy samples were sent to the University of Rochester's Department of Pathology for analysis ordered by the referring physician. Each specimen was scored for steatosis according to [Kleiner et al. \(2005\)](#) and [Angulo et al. \(2015\)](#). In addition, a conventional fibrosis score was assessed on a scale of F0–F4 (where F4 indicates severe/cirrhosis).

Statistics

Because the fibrosis and steatosis scores are semi-quantitative, Spearman's rank correlation coefficient was used as a non-parametric measure of rank correlation (see [Table 1](#)). Linear correlations were also examined and reported as Pearson's correlations. As in [Nightingale et al. \(2015\)](#), the ability to distinguish disease states was evaluated by performing receiver operating characteristic (ROC) curve analysis ([Zweig and Campbell 1993](#); [Fawcett 2004](#)). For fibrosis staging, ROC curves were constructed corresponding to the separation of patients from mild, moderate and advanced fibrosis, with stages $\geq F1$, $\geq F2$ and $\geq F3$, respectively. For steatosis scoring, patients were separated into groups with no steatosis, low steatosis and high steatosis, with

grades $\geq S0$, $\geq S1$ and $\geq S2$, respectively. ROC curves were constructed for four metrics: group SWS, SWD, PLC and SWA. The area under the ROC curve (AUROC) quantifies the ability to distinguish between disease states.

RESULTS

Oil-in-gel custom-made phantoms

It was found previously ([Parker et al. 2018b](#)) that as oil-in-gelatin suspensions increase in oil volume from 2%–36%, the general trend is toward decreased stress relaxation force and, consequently, decreased shear modulus at low frequencies, consistent with earlier studies ([Nguyen et al. 2014](#)).

For this study, the values of dispersion and PLC have been estimated and added to the previously reported data, as summarized in [Figure 4](#). It can be observed that the linear dispersion slope and the power law parameter increased monotonically with the volume percentage of oil, with reasonable agreement between the mechanical measurements and SWE results. Moreover, the independent predictions of SWA obtained from the KVFD model, the SWE measurements and the

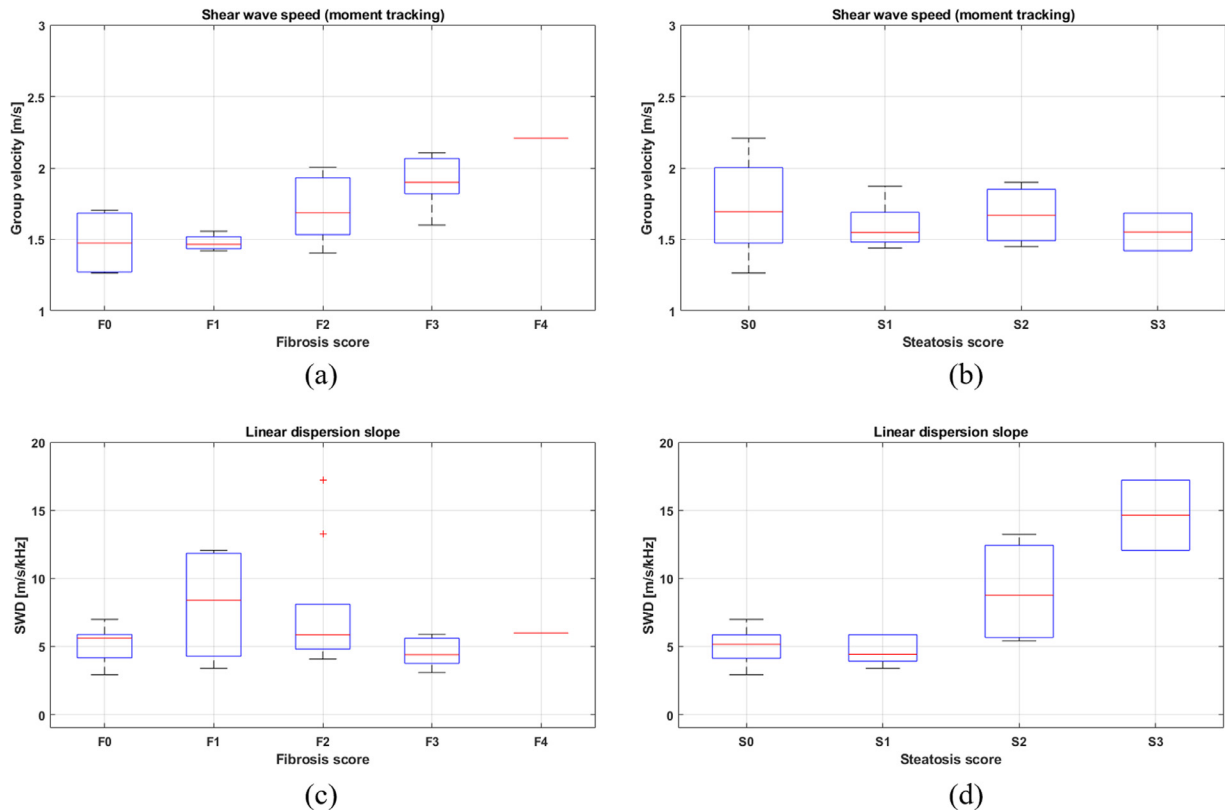


Fig. 5. Shear wave speed (SWS) and shear wave dispersion (SWD) results as a function of fibrosis scores (left column) and steatosis scores (right column). Spearman's (and Pearson's) rank statistical analysis confirmed the trend of increasing SWS with increased fibrosis and increasing SWD with increased steatosis.

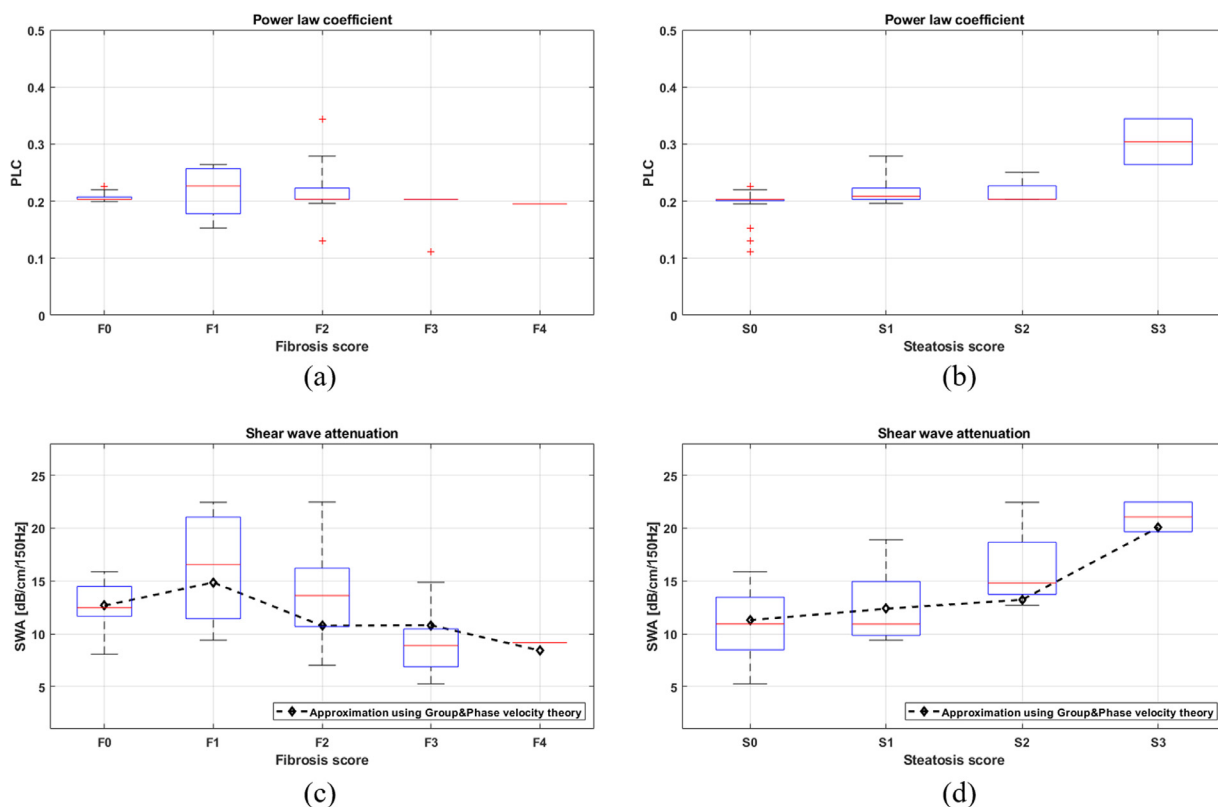


Fig. 6. Power law coefficient (PLC) and shear wave attenuation (SWA) results as a function of fibrosis scores (left column) and steatosis scores (right column). Spearman's (and Pearson's) rank statistical analysis confirmed the trend of increasing PLC and SWA with increased steatosis. Additionally, good agreement was obtained between the SWA results obtained using the method proposed in Parker et al. (2018a, 2018b) and the approximation based on eqns (5) and (6) for both fibrosis (c) and steatosis (d) scores.

approximation using eqns (5) and (6) have similar trends. Thus, the relationship between SWD and SWA under a power law mode seems to be appropriate and useful for this inhomogeneous, composite phantom.

In vivo liver tissue

Figures 5 and 6 illustrate the elastography results reporting SWS, SWD and PLC, SWA as a function of fibrosis and steatosis scores, respectively. The SWS and SWA results were reported previously in Sharma et al. (2019), and now the measured SWD and PLC results are also included. Across the population studied, SWS varied from 1.2–2.5 m/s, SWD varied from 3–18 m/s/kHz, PLC varied from 0.1–0.3 and SWA varied from 5–25 dB/cm. For SWD, PLC and SWA, the lower values are associated with non-steatotic livers, as illustrated in Figures 5d, 6b and 6d, respectively. Furthermore, SWA results using the method reported in Parker et al. (2018a) and the approximation based on eqns (5) and (6) are compared for both fibrosis in Figure 6c and steatosis scores in Figure 6d, with reasonable agreement between both results. Spearman's and Pearson's rank correlation values are summarized in Table 1 and suggest that SWS

increases with fibrosis score, whereas SWD, PLC and SWA increase with steatosis score.

In addition to previous analysis, the AUROC curves were obtained using different thresholds for each elastography parameter as shown in Figures 7 and 8. Results confirm that better performance is obtained for SWS as a function of fibrosis scores, whereas SWD and SWA as a function of steatosis scores. Despite the tight theoretical link between PLC and SWA, the performance of PLC with respect to fibrosis or steatosis is not clear when the threshold is fixed at moderate fibrosis or steatosis (AUCROC equals to 0.76 for both cases). More experiments are needed to determine if the PLC could also be used to differentiate fibrosis scores.

DISCUSSION

The focus of this study was to characterize different viscoelastic materials measuring SWS (group and phase), SWD, PLC and SWA as a function of viscosity (higher percentages of oil-in-gelatin phantoms and steatosis stages in *in vivo* liver). In many previous elastographic studies, SWS was the primary parameter.

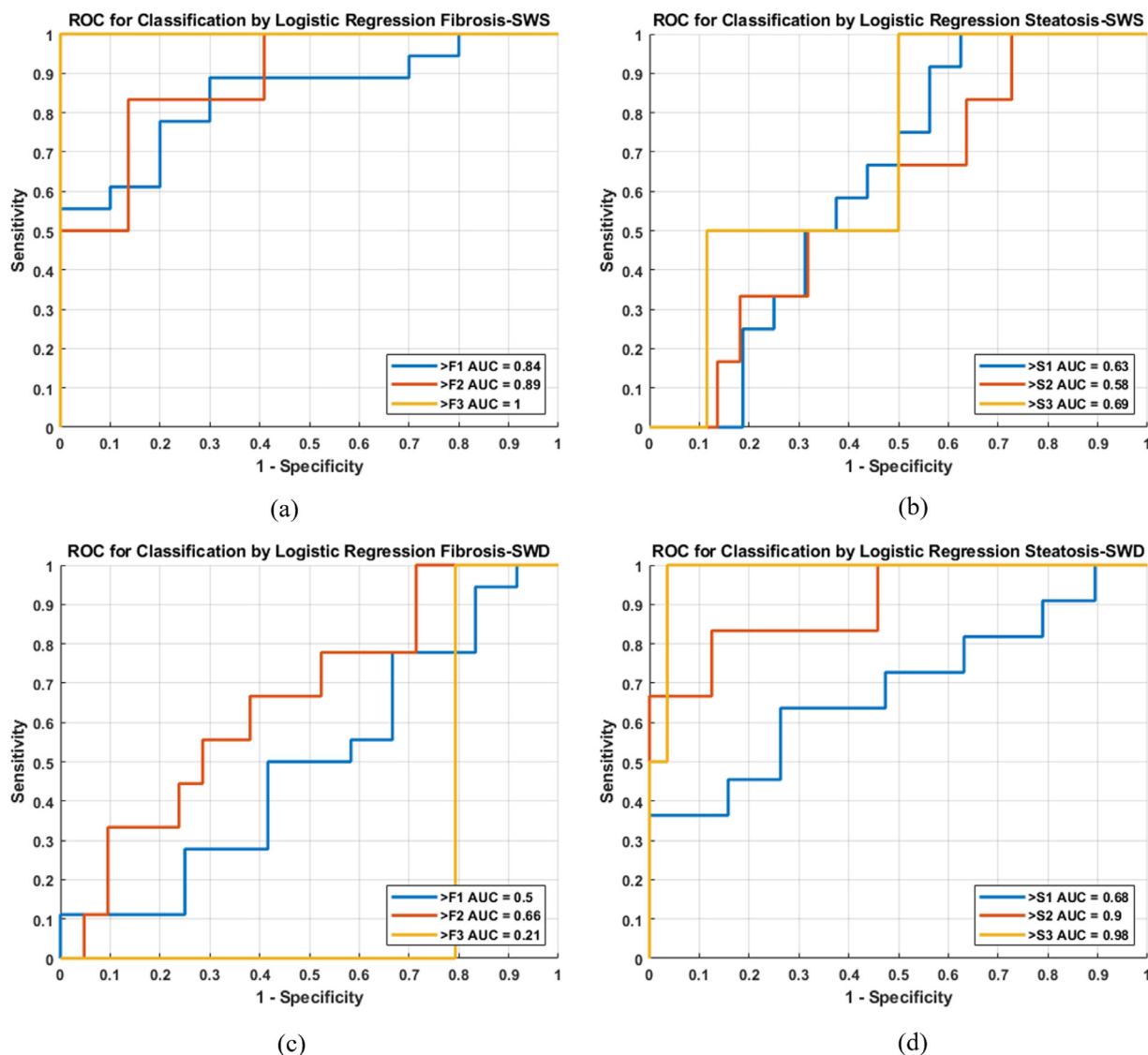


Fig. 7. Receiver operating characteristic (ROC) curves for SWS and SWD parameters for fibrosis (left column) and steatosis (right column). ROC curves were constructed corresponding to the separation of patients into mild, moderate and advanced fibrosis and into groups with low steatosis and high steatosis with grades. Area under the ROC curve (AUROC) values are reported at each threshold used in ROC curves to quantify the ability to distinguish between disease states.

However, the inter-relationship between dispersion of SWS versus frequency and attenuation and particular power law forms has not been extensively probed in phantoms and *in vivo* tissue (Futterman 1962; Waters et al. 2000, 2005; Mobley et al. 2003). Thus, this study experimentally verifies that the SWD in an individual material or liver is linked to the SWA (lossy, viscoelastic nature of the tissue).

The SWD value has been used, together with SWS, to predict the shear and viscoelastic moduli using a rheological model (*i.e.*, Voigt, Kelvin–Voigt models). Deffeux et al. (2015) evaluated 120 liver cases, measuring SWD to estimate viscosity, and concluded that viscosity

is a poor predictor for steatosis staging. Their work indicated a different trend compared with the results obtained in this study for SWD and its relationship with liver steatosis. However, Sugimoto et al. (2020) indicated that this discrepancy, compared with other clinical results (and ours now), may be owing to the different population characteristics and etiologies in patients studied by Deffeux et al. (2015). Another study reported by Chen et al. (2013) estimated viscosity in 35 patients and illustrated that viscosity was a less predictive value for liver stiffness and fibrosis staging. This study did not include an analysis of viscosity and its usefulness for steatosis evaluation.

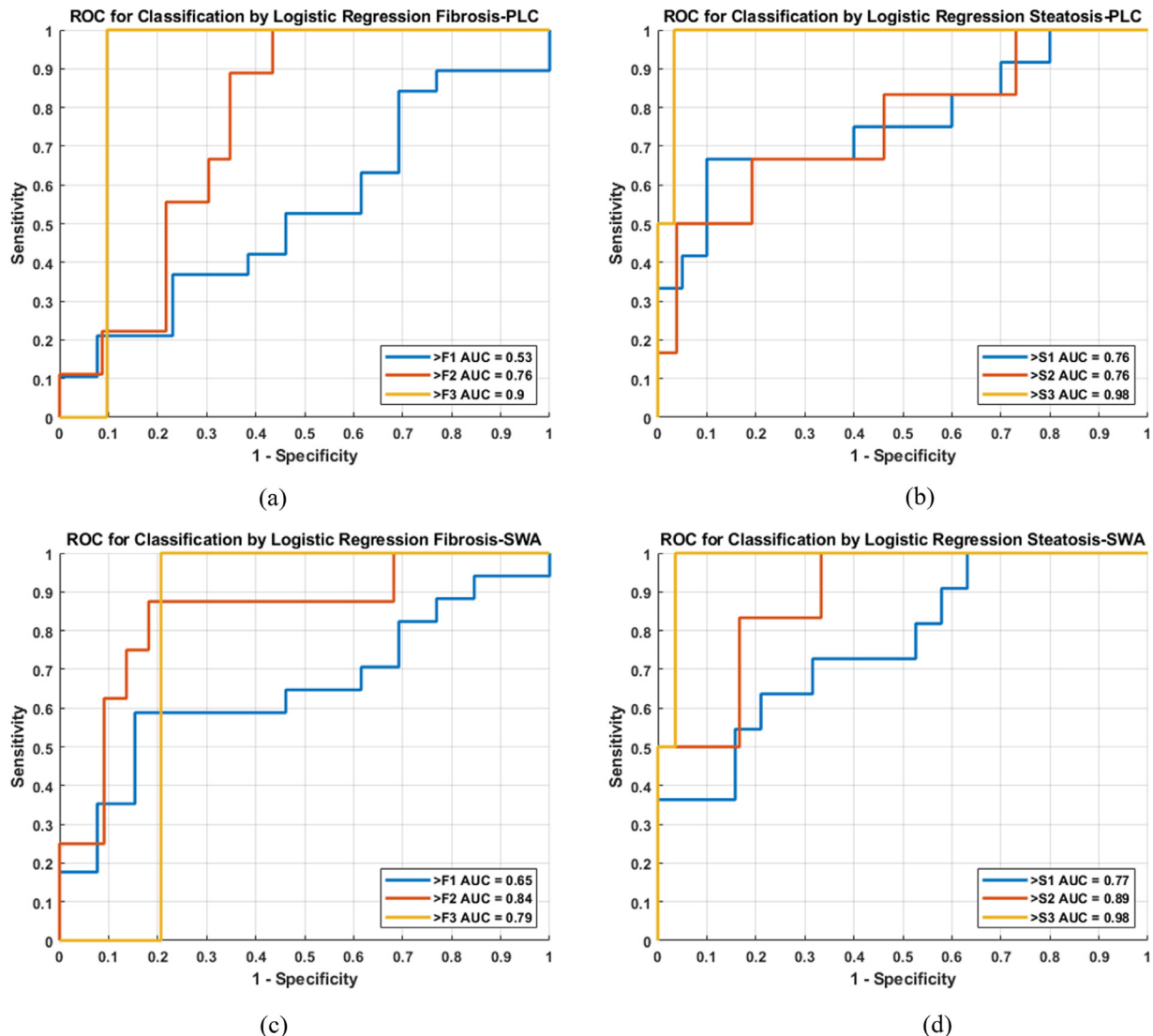


Fig. 8. Receiver operating characteristic (ROC) curves for power law coefficient (PLC) and shear wave attenuation (SWA) parameters for fibrosis (left column) and steatosis (right column). ROC curves were constructed corresponding to the separation of patients with mild, moderate and advanced fibrosis and into groups with low steatosis and high steatosis with grades. Area under the ROC curve (AUROC) values are reported at each threshold used in ROC curves to quantify the ability to distinguish between disease states.

Figure 9 summarizes the range of different estimates for SWD, as a function of frequency range, from reports on human liver experiments using a variety of techniques. These SWD results were obtained using ARF and harmonic-based elastography methods using ultrasound and magnetic resonance imaging. Each clinical study reported SWD based on different frequency ranges. SWD estimates are illustrated by each study's mean reported values. Some of these studies did not report the frequency range (illustrated in Fig. 9). Thus, we selected 100–300 Hz as a reference frequency range for all of these cases mainly for two reasons: these studies used the same ultrasound equipment (*i.e.*, Aplio i800,

Canon Medical Systems), and all used ARF-based SWE, a method where the propagating shear wave frequency range (Deffieux et al. 2009) is typically in the low hundred(s) of hertz. Figure 9 clearly depicts the wide range of estimates among different methods. Creating a more uniform and device-independent set of measurements for clinicians will clearly require a reconciliation of differences and sources of disagreement, among these are the different shear wave frequencies used to measure the SWD along with other experimental factors.

Similarly for SWA, some studies have reported results at one specific frequency: 100 Hz (Parker et al. 2018a, 2018b), 150 Hz (Sharma et al. 2019). Other studies have

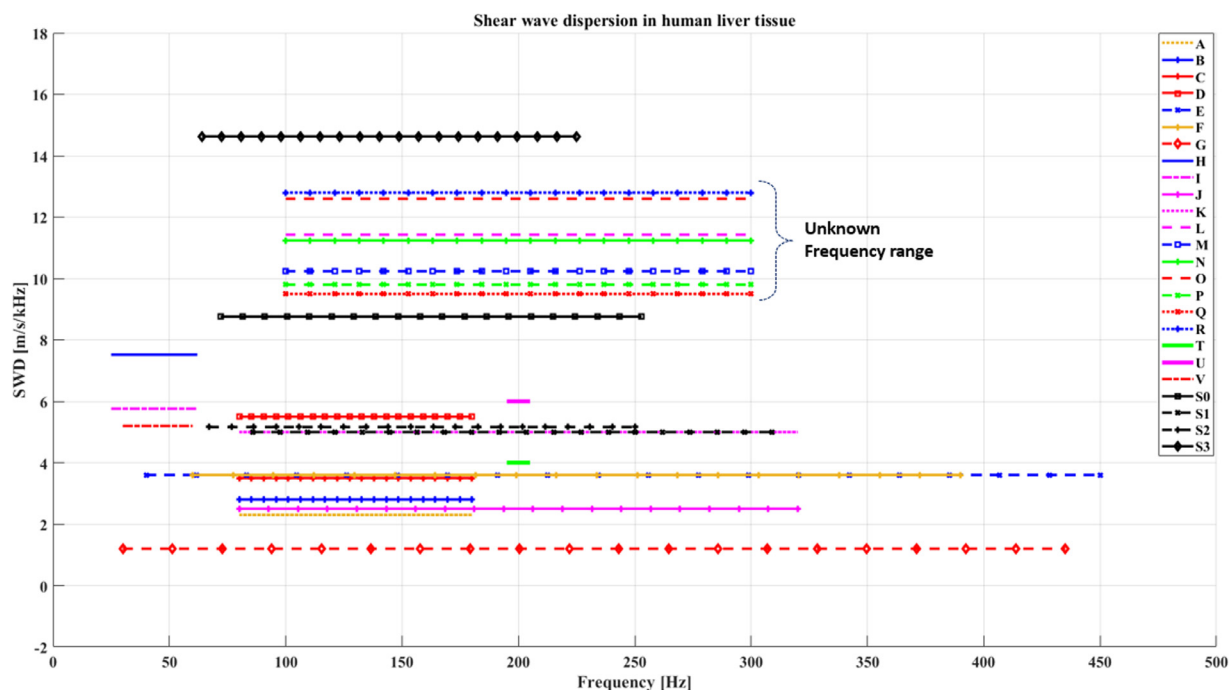


Fig. 9. Literature summary of shear wave dispersion studies on human liver tissue. The y -axis represents the mean reported dispersion in $\text{m/s}/100 \text{ Hz}$. The shaded vertical bars represent the standard deviation values reported in each study. The x -axis represents the frequency range used to measure the shear wave dispersion (SWD). (a) *Ex vivo* normal human liver (Barry et al. 2012). (b) *Ex vivo* human liver, 10% fat (Barry et al. 2012). (c) *Ex vivo* human liver, 10% fat + fibrosis (Barry et al. 2012). (d) *Ex vivo* human liver, 10% fat + cirrhosis (Barry et al. 2012). (e) Healthy liver (Defieux et al. 2009). (f) Healthy liver (Muller et al. 2009). (g) Liver fibrosis F1 (Bavu et al. 2011). (h) Healthy liver (Klatt et al. 2007). (i) Healthy liver (Asbach et al. 2008). (j) Thin patient (Ormachea et al. 2019). (k) Obese patient (Ormachea et al. 2019). (l) Healthy liver in children (Trout et al. 2020). (m) Healthy liver in adults (Trout et al. 2020). (n) Healthy liver in adults (Yoo et al. 2019). (o) With necro-inflammation (Lee et al. 2019). (p) Without necro-inflammation (Lee et al. 2019). (q) Lobular inflammation, grade I (Sugimoto et al. 2018). (r) Lobular inflammation, grade II (Sugimoto et al. 2018). (t) non-alcoholic fatty liver disease <F2 stage (Nightingale et al. 2015). (u) Non-alcoholic fatty liver disease >F3 stage (Nightingale et al. 2015). (v) Volunteers (Tzschatzsch et al. 2015). S0, S1, S2 and S3 illustrates the SWD results in this study as a function of steatosis score.

reported results at different frequencies: 140–220 Hz (Budelli et al. 2017), 100–300 Hz (Nenadic et al. 2017). For shear wave packets generated from push pulses, the frequency band chosen to take measurements can have a strong influence on the experimental results (Parker et al. 2018a, 2018b). The issues of shear wave frequencies are discussed in more detail in the Appendix.

Ultimately, confusion or disagreement between different elastography results can be caused by the choice of experimental conditions: frequency range and measurement type, group velocity versus phase velocity, SWD or SWA. This study attempts to resolve this problem by measuring all elastography parameters over frequency ranges that fairly overlap among the phantom or the clinical experiments and by illustrating their inter-relationships.

As mentioned in Sharma et al. (2019), at this time it is unknown how many biological co-factors (besides steatosis) may increase or decrease SWD, PLC and SWA in the liver. Nevertheless, some recent studies

indicate that SWD is related to liver inflammation (Sugimoto et al. 2020); liver transplant rejection cases had a lower SWA than normal livers (Nenadic et al. 2017). As in our phantom study, Bernard et al. (2017) found a doubling of attenuation in 20% oil-in-gelatin phantoms compared with the baseline case of 0% oil. Thus, the phantom studies reported previously reveal a subtle increase in SWD, PLC and SWA for low concentrations of oil (<20% by volume) and with increasing rates of change thereafter, suggesting that the measurement of these parameters will be most useful for the higher viscosity levels and steatotic grades in liver, but more difficult to distinguish in the early low grades. This appears to be consistent with the results illustrated in Figures 5 and 6. Further study is required to establish the mechanisms of any co-factors. Finally, in addition to biological co-factors the measured parameters can be influenced by the presence of boundaries and small geometries. Shear waves in plates and rods (Graff 1975) have more

complicated dispersion curves because of shape and boundary effects, and so general conclusions based on eqns (5) and (6) or liver results will not necessarily apply to tendons, for example.

CONCLUSIONS

A comprehensive viscoelastic characterization, using SWE, was attained in viscoelastic phantoms and *in vivo* liver tissue, indicating consistent inter-relationships and reasonable agreement with independent measurements. It was experimentally confirmed that SWD and SWA are linked and can be used to assess material or tissue viscosity changes, with relatively simple interrelationships as long as these materials are reasonably approximated by a power law rheological model. This preliminary study indicates the possible utility of SWD and attenuation in non-invasive and quantitative measurement of steatosis.

Acknowledgments—We are grateful for support from Samsung Medison and for the loan of equipment. We also thank Dr. D. Rubens and Dr. A. Sharma for clinical data acquisition and Dr. Z. Hah for his technical support and suggestions.

Conflict of Interest—The authors declare that the research was conducted in the absence of any commercial or financial relationships that could be construed as a potential conflict of interest.

SUPPLEMENTARY MATERIALS

Supplementary material associated with this article can be found in the online version at doi:10.1016/j.ultrasmedbio.2020.08.023.

REFERENCES

- Angulo P, Kleiner DE, Dam-Larsen S, Adams LA, Bjornsson ES, Charatcharoenwithaya P, Mills PR, Keach JC, Lafferty HD, Stahler A, Hafidatottir S, Bendtsen F. Liver fibrosis, but no other histologic features, is associated with long-term outcomes of patients with nonalcoholic fatty liver disease. *Gastroenterology* 2015;149:389–397.e10.
- Asbach P, Klatt D, Hamhaber U, Braun J, Somasundaram R, Hamm B, Sack I. Assessment of liver viscoelasticity using multifrequency MR elastography. *Magn Reson Med* 2008;60:373–379.
- Baddour N. Multidimensional wave field signal theory: Mathematical foundations. *AIP Adv* 2011;1:022120.
- Baddour N. Multidimensional wave field signal theory: Transfer function relationships. *Math Probl Eng* 2012;2012:478295.
- Barry CT, Mills B, Hah Z, Mooney RA, Ryan CK, Rubens DJ, Parker KJ. Shear wave dispersion measures liver steatosis. *Ultrasound Med Biol* 2012;38:175–182.
- Bavu E, Gennisson JL, Couade M, Bercoff J, Mallet V, Fink M, Badel A, Vallet-Pichard A, Nalpas B, Tanter M, Pol S. Noninvasive *in vivo* liver fibrosis evaluation using supersonic shear imaging: A clinical study on 113 hepatitis C virus patients. *Ultrasound Med Biol* 2011;37:1361–1373.
- Bernard S, Kazemirad S, Cloutier G. A frequency-shift method to measure shear-wave attenuation in soft tissues. *IEEE Trans Ultrason Ferroelectr Freq Control* 2017;64:514–524.
- Budelli E, Brum J, Bernal M, Deffieux T, Tanter M, Lema P, Negreira C, Gennisson JL. A diffraction correction for storage and loss moduli imaging using radiation force based elastography. *Phys Med Biol* 2017;62:91–106.
- Chen W, Holm S. Modified Szabo's wave equation models for lossy media obeying frequency power law. *J Acoust Soc Am* 2003;114:2570–2574.
- Chen S, Fatemi M, Greenleaf JF. Quantifying elasticity and viscosity from measurement of shear wave speed dispersion. *J Acoust Soc Am* 2004;115:2781–2785.
- Chen SG, Sanchez W, Callstrom MR, Gorman B, Lewis JT, Sanderson SO, Greenleaf JF, Xie H, Shi Y, Pashley M, Shamdasani V, Lachman M, Metz S. Assessment of liver viscoelasticity by using shear waves induced by ultrasound radiation force. *Radiology* 2013;266:964–970.
- Deffieux T, Montaldo G, Tanter M, Fink M. Shear wave spectroscopy for *in vivo* quantification of human soft tissues visco-elasticity. *IEEE Trans Med Imaging* 2009;28:313–322.
- Deffieux T, Gennisson JL, Bousquet L, Corouge M, Coscinea S, Amroun D, Tripon S, Terris B, Mallet V, Sogni P, Tanter M, Pol S. Investigating liver stiffness and viscosity for fibrosis, steatosis and activity staging using shear wave elastography. *J Hepatol* 2015;62:317–324.
- Fawcett T. ROC graphs: Notes and practical considerations for researchers. *Mach Learn* 2004;31:1–38.
- Futterman WL. Dispersive body waves. *J Geophys Res* 1962;67:5279–5291.
- Graff KF. Wave motion in elastic solids. Oxford: Clarendon Press; 1975.
- Holm S. Waves with power-law attenuation. Cham: Springer and ASA Press; 2019.
- Klatt D, Hamhaber U, Asbach P, Braun J, Sack I. Noninvasive assessment of the rheological behavior of human organs using multifrequency MR elastography: A study of brain and liver viscoelasticity. *Phys Med Biol* 2007;52:7281–7294.
- Kleiner DE, Brunt EM, Van Natta M, Behling C, Contos MJ, Cummings OW, Ferrell LD, Liu YC, Torbenson MS, Unalp-Arida A, Yeh M, McCullough AJ, Sanyal AJ, Nonalcoholic Steatohepatitis Clinical Research Network. Design and validation of a histological scoring system for nonalcoholic fatty liver disease. *Hepatology* 2005;41:1313–1321.
- Kumar V, Denis M, Gregory A, Bayat M, Mehrmohammadi M, Fazzio R, Fatemi M, Alizad A. Viscoelastic parameters as discriminators of breast masses: Initial human study results. *PLoS One* 2018;13:e0205717.
- Lee DH, Lee JY, Bae JS, Yi NJ, Lee KW, Suh KS, Kim H, Lee KB, Han JK. Shear-wave dispersion slope from US shear-wave elastography: Detection of allograft damage after liver transplantation. *Radiology* 2019;293:327–333.
- Mobley J, Waters KR, Miller JG. Finite-bandwidth effects on the causal prediction of ultrasonic attenuation of the power-law form. *J Acoust Soc Am* 2003;114:2782–2790.
- Muller M, Gennisson JL, Deffieux T, Tanter M, Fink M. Quantitative viscoelasticity mapping of human liver using supersonic shear imaging: Preliminary *in vivo* feasibility study. *Ultrasound Med Biol* 2009;35:219–229.
- Nenadic I, Urban MW, Qiang B, Chen S, Greenleaf J. Model-free quantification of shear wave velocity and attenuation in tissues and its *in vivo* application. *J Acoust Soc Am* 2013;134:4011–4011.
- Nenadic IZ, Qiang B, Urban MW, Zhao H, Sanchez W, Greenleaf JF, Chen S. Attenuation measuring ultrasound shearwave elastography and *in vivo* application in post-transplant liver patients. *Phys Med Biol* 2017;62:484.
- Nguyen MM, Zhou S, Robert JL, Shamdasani V, Xie H. Development of oil-in-gelatin phantoms for viscoelasticity measurement in ultrasound shear wave elastography. *Ultrasound Med Biol* 2014;40:168–176.
- Nightingale KR, Rouze NC, Rosenzweig SJ, Wang MH, Abdelmalek MF, Guy CD, Palmeri ML. Derivation and analysis of viscoelastic properties in human liver: Impact of frequency on fibrosis and steatosis staging. *IEEE Trans Ultrason Ferroelectr Freq Control* 2015;62:165–175.
- Ormaechea J, Lavarello RJ, McAleavey SA, Parker KJ, Castaneda B. Shear Wave Speed Measurements Using Crawling Wave Sonoelastography and Single Tracking Location Shear Wave Elasticity

- Imaging for Tissue Characterization. *IEEE Trans Ultrason Ferroelectr Freq Control* 2016;63:1351–1360.
- Ormachea J, Parker KJ, Barr RG. An initial study of complete 2D shear wave dispersion images using a reverberant shear wave field. *Phys Med Biol* 2019;64 145009.
- Papoulis A. *The Fourier integral and its applications*, Ch. 2. New York: McGraw-Hill; 1987.
- Parker KJ. Real and causal hysteresis elements. *J Acoust Soc Am* 2014;135:3381–3389.
- Parker KJ, Baddour N. The Gaussian shear wave in a dispersive medium. *Ultrasound Med Biol* 2014;40:675–684.
- Parker KJ, Ormachea J, Drage MG, Kim H, Hah Z. The biomechanics of simple steatosis and steatohepatitis. *Phys Med Biol* 2018;63 105013.
- Parker KJ, Ormachea J, Hah Z. Group versus phase velocity of shear waves in soft tissues. *Ultrason Imaging* 2018;40:343–356.
- Parker KJ, Ormachea J, Will S, Hah Z. Analysis of transient shear wave in lossy media. *Ultrasound Med Biol* 2018;44:1504–1515.
- Parker KJ, Szabo T, Holm S. Towards a consensus on rheological models for elastography in soft tissues. *Phys Med Biol* 2019;64 215012.
- Sharma AK, Reis J, Oppenheimer DC, Rubens DJ, Ormachea J, Hah Z, Parker KJ. Attenuation of shear waves in normal and steatotic livers. *Ultrasound Med Biol* 2019;45:895–901.
- Sugimoto K, Moriyasu F, Oshiro H, Yoshimasu Y, Takeuchi H, Kasai Y, Furuichi Y, Itoi T. Value of viscosity and viscoelasticity measurement in patients with NAFLD using shear wave ultrasound elastography. *Kanzo* 2018;59:370–373.
- Sugimoto K, Moriyasu F, Oshiro H, Takeuchi H, Yoshimasu Y, Kasai Y, Itoi T. Clinical utilization of shear wave dispersion imaging in diffuse liver disease. *Ultrasonography* 2020;39:3–10.
- Szabo TL. Causal theories and data for acoustic attenuation obeying a frequency power-law. *J Acoust Soc Am* 1995;97:14–24.
- Trout AT, Xanthakos SA, Bennett PS, Dillman JR. Liver shear wave speed and other quantitative ultrasound measures of liver parenchyma: Prospective evaluation in healthy children and adults. *AJR Am J Roentgenol* 2020;214:557–565.
- Tzschatzsch H, Ipek-Ugay S, Trong MN, Guo J, Eggers J, Gentz E, Fischer T, Schultz M, Braun J, Sack I. Multifrequency time-harmonic elastography for the measurement of liver viscoelasticity in large tissue windows. *Ultrasound Med Biol* 2015;41:724–733.
- Urban MW, Chen J, Ehman RL. Comparison of shear velocity dispersion in viscoelastic phantoms measured by ultrasound-based shear wave elastography and magnetic resonance elastography. In: *Proceedings, 2017 IEEE International Ultrasonics Symposium (IUS)*, Washington, DC. Piscataway, NJ. : IEEE; 2017.
- Waters KR, Hughes MS, Mobley J, Brandenburger GH, Miller JG. On the applicability of Kramers-Kronig relations for ultrasonic attenuation obeying a frequency power law. *J Acoust Soc Am* 2000;108:556–563.
- Waters KR, Mobley J, Miller JG. Causality-imposed (Kramers-Kronig) relationships between attenuation and dispersion. *IEEE Trans Ultrason Ferroelectr Freq Control* 2005;52:822–823.
- Yoo J, Lee JM, Joo I, Lee DH, Yoon JH, Kang HJ, Ahn SJ. Prospective validation of repeatability of shear wave dispersion imaging for evaluation of non-alcoholic fatty liver disease. *Ultrasound Med Biol* 2019;45:2688–2696.
- Zhang M, Castaneda B, Wu Z, Nigwekar P, Joseph JV, Rubens DJ, Parker KJ. Congruence of imaging estimators and mechanical measurements of viscoelastic properties of soft tissues. *Ultrasound Med Biol* 2007;33:1617–1631.
- Zweig MH, Campbell G. Receiver-operating characteristic (ROC) plots: A fundamental evaluation tool in clinical medicine. *Clin Chem* 1993;39:561–577.